Effect of the planet shine on the corona : Application to the Martian hot oxygen

Jean-Yves Chaufray, Justin Deighan, A. Ian F. Stewart, Nicholas Schneider, John Clarke, François Leblanc, Bruce Jakosky

HAL Id: insu-01389787

https://insu.hal.science/insu-01389787

Submitted on 16 Jan 2017

RESEARCH ARTICLE

Special Section:
Major Results From the MAVEN Mission to Mars

Key Points:
- Quantify the effect of the backscattered photons on the hot oxygen brightness
- The nightside volume emission rate of the cold oxygen is modified by the presence of an extended hot oxygen corona
- Analytical formulation to take into account the variations with the hot oxygen temperature is proposed

Correspondence to:
J.-Y. Chaufray,
jean-yves.chaufray@latmos.ipsl.fr

Effect of the planet shine on the corona: Application to the Martian hot oxygen

J.-Y. Chaufray[1], J. Deighan[2], A. I. F. Stewart[2], N. Schneider[2], J. Clarke[3], F. Leblanc[1], and B. Jakosky[2]

[1]LATMOS/IPSL, UPMC Université Paris 06, Sorbonne Universités, UVSQ, CNRS, Paris, France, [2]LASP, University of Colorado Boulder, Boulder, Colorado, USA, [3]Center for Space Physics, Boston University, Boston, Massachussetts, USA

Abstract Systematic observations of the Martian hot oxygen corona by Imaging Ultraviolet Spectrograph on Mars Atmosphere and Volatile and EvolutioN can be used to constrain estimates of the current neutral oxygen escape rate. In this paper, we investigate the effect of the photons emitted from the thermosphere and lower exosphere on the emissivity of the hot oxygen corona at 130.4 nm. We compare this source of illumination, generally neglected, to the direct solar illumination used to convert the O I 130.4 triplet brightness into line-of-sight column density. This study is performed using a radiative transfer model with two Maxwellian oxygen populations, assuming spherical symmetry for the cold and hot oxygen densities. Contribution to the corona from the illumination of the exosphere by the sunlit atmosphere depends on the amount of cold oxygen and varies with altitude and solar zenith angle. An analytic formulation to take into account variations of this effect with respect to the hot oxygen kinetic temperature is proposed. The effect of the atmosphere sunlit should be general and occur on other planets for other very optically thick resonance lines.

1. Introduction

Nonthermal escape of atomic oxygen from Mars has been hypothesized from photochemical considerations [*McElroy*, 1972]. The O_2^+ ion is the main ion in the Martian ionosphere [*Hanson et al.*, 1977; *Bougher et al.*, 2015] and is formed from the chemical reactions between the primary ion CO_2^+ and atomic oxygen: $CO_2^+ + O \rightarrow O_2^+ + CO$. This ion is mainly lost by dissociative recombination: $O_2^+ + e- \rightarrow O + O$. This reaction is exothermic and the two oxygen atoms can have a velocity larger than the Martian escape velocity. Therefore, these hot oxygen atoms produced in the rarefied region of the Martian upper atmosphere can escape from Mars or have large ballistic trajectories leading to the formation of an extended oxygen distribution around Mars.

According to most models [e.g., *Yagi et al.*, 2012; *Lee et al.*, 2015], the oxygen density below 500 km is due to the diffusion/ballistic movement of the oxygen atoms produced in the lower thermosphere and characterized by Maxwellian velocity distribution at the atmospheric temperature: the "thermal oxygen population." Above 500 km, the contribution from the dissociative recombination of O_2^+ to the total oxygen density becomes important [*Yagi et al.*, 2012; *Lee et al.*, 2015]. A hot oxygen corona has been observed on Venus by the Pioneer Venus Orbiter [*Nagy et al.*, 1981] through the resonant scattering of the solar photons by the energetic oxygen atoms. On Mars, it is only recently that this hot oxygen component has been observed.

The first detection of the hot oxygen corona around Mars was performed by the UV spectrograph Alice aboard Rosetta during its flyby of Mars in 2007 [*Feldman et al.*, 2011] and by the Hubble Space Telescope [*Carveth et al.*, 2012]. More systematic observations with a much better vertical resolution are now acquired by the instrument Imaging Ultraviolet Spectrograph (IUVS) aboard Mars Atmosphere and Volatile and EvolutioN (MAVEN) [*Deighan et al.*, 2015]. The observations from IUVS/MAVEN confirmed a transition from a cold oxygen corona [*Chaufray et al.*, 2015a] to a hot oxygen corona near 600 km [*Deighan et al.*, 2015]. This transition is suggested by the change of the brightness scale height from being consistent with the ambient temperature to having a slope corresponding to an O atom energy of 1.1 eV between 1000 and 3500 km [*Deighan et al.*, 2015].

Other processes such as sputtering [*Leblanc et al.*, 2015] could also be a source of hot oxygen around Mars. However, the decrease of the hot oxygen corona with the solar zenith angle [*Lee et al.*, 2015], its correlation with the solar ionizing flux [*Deighan et al.*, 2015], as well as the current nondetection of variations of the hot oxygen corona with respect to the pick up ions precipitating flux suggest that the contribution of the sputtering to the hot oxygen corona is minor at present solar conditions at Mars, in agreement with models [*Chaufray et al.*, 2007].

The typical intensity of the observed O 130.4 nm triplet above 500 km is of few Rayleighs [*Feldman et al.*, 2011; *Deighan et al.*, 2015], too weak to be observed by the UV spectrograph SPICAM on Mars Express [*Chaufray et al.*, 2009]. This low brightness is due to the low density of oxygen above 500 km. Because of this low density the optically thin assumption is generally used and the line-of-sight column density converted into brightness using the solar excitation frequency (*g* factor) [*Feldman et al.*, 2011; *Lee et al.*, 2015]. Such an assumption is probably correct to derive a first estimate. However, for an accurate estimate, the photons scattered or emitted at lower altitudes should be also considered. The goal of this study is to quantify this "Mars shine" effect using a radiative transfer model with two oxygen populations. One population called the cold population dominant in the thermosphere and lower exosphere, and one hot population assumed to have a Maxwellian velocity distribution but with a kinetic temperature much larger than the Martian thermosphere/lower exosphere. The radiative transfer model as well as the oxygen density profiles used as input of the models are described in section 2. The change of the cold oxygen volume emission rate due to the presence of the hot oxygen population is described in section 3, whereas the change of the hot oxygen volume emission rate due to the presence of the cold population is described in section 4 and is followed by a conclusion in section 5.

2. Models

Because the goal of this paper is to analyze the consequences of the atmosphere sunlit when interpreting the hot oxygen corona and not to study the variability of the hot oxygen corona, we will use spherically symmetric cold and hot oxygen densities. While most models predict a 3-D structure for both cold [e.g., *Gonzalez-Galindo et al.*, 2009, 2015; *Valeille et al.*, 2009a] and hot oxygen densities [*Valeille et al.* 2009b; *Yagi et al.*, 2012], this assumption is sufficient to estimate the effects of the scattered photons in the thermosphere/low exosphere on the hot oxygen corona.

2.1. Thermospheric Density

The approach is similar to the one described in *Chaufray et al.* [2009]. The temperature profile below 200 km is parameterized by the value of the temperature at 200 km using the formulation of *Krasnopolsky* [2002]. We consider only two species: O and CO_2. The total density $O + CO_2$ is derived from the hydrostatic equation. The diffusion equation is solved in combination with the hydrostatic equation to derive the density of O and CO_2 at different altitudes. The CO_2 density at 80 km is fixed to 2.6×10^{13} cm^{-3} [*Krasnopolsky*, 2002]. The thermal oxygen thermospheric density depends only on two parameters: O density at 80 km and temperature at exobase. Below 80 km, we assume the atmosphere to be fully opaque to the photons at 130.4 nm.

2.2. Exospheric Density

The CO_2 density does not need to be described in the exosphere because the absorption of the emission by CO_2 is negligible at these altitudes. The cold oxygen density is computed using a Chamberlain approach [*Chamberlain*, 1963] and therefore depends only on two parameters: oxygen density at the exobase and temperature at the exobase.

The hot oxygen density is only computed above the exobase. Here, again, we use a Chamberlain approach but for temperature much larger than the atmospheric temperature at the exobase. Typical temperature from 1000 to 10,000 K as suggested by models and observations from Rosetta and MAVEN and the density at 200 km [*Feldman et al.*, 2011; *Deighan et al.*, 2015]. The hot oxygen density at 200 km is chosen to have a density profile above 500 km close to the estimated densities [*Lee et al.*, 2015]. We assume a uniform temperature for the hot oxygen population. Several processes could contribute to the hot oxygen density, but the scale heights of the hot oxygen density from each process are very similar [*Groller et al.*, 2014], and therefore, our single-scale height assumption should still be valid.

Examples of vertical oxygen distribution of the cold and hot oxygen densities are displayed in Figure 1. These cold density profiles correspond to an exospheric temperature of 300 K and an oxygen density at 200 km of 1×10^7, 2.0×10^7, 4.5×10^7, and 1×10^8 cm^{-3} encompassing the values derived from different measurements [*Chaufray et al.*, 2009, 2015a; *Feldman et al.*, 2011; *Bougher et al.*, 2015]. The hot oxygen density profiles are chosen to encompass the hot oxygen densities derived from observations and models [*Feldman et al.*, 2011; *Lee et al.*, 2015].
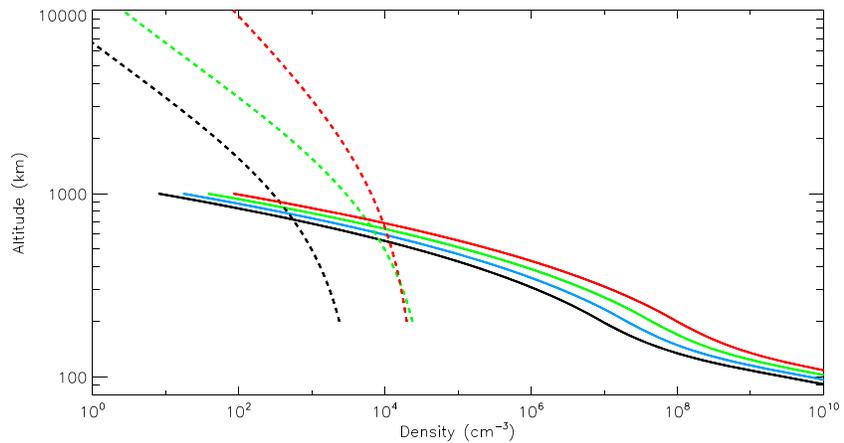
Figure 1. Examples of cold oxygen density profiles (solid lines) and hot oxygen density profile (dashed lines) used as input of the radiative transfer model. The cold oxygen profile has been derived using an exospheric temperature of 300 K, while different scale heights (~300 km for the black and green profiles and ~1200 km for the red profile) are used to simulate the hot oxygen corona.

2.3. Radiative Transfer Model

The radiative transfer model is that used by *Chaufray et al.* [2015a] to analyze the first observations of the cold oxygen corona by IUVS/MAVEN, but extended to include two different oxygen populations, similar to the model used to study the Venusian hydrogen nightside corona [*Chaufray et al.*, 2015b]. This model is based on a Monte Carlo approach following the trajectories of test photons from the Sun to the Martian atmosphere. Each solar line of the 130.4 nm triplet at Mars is approximated by a flat "boxcar" line shape with a 10 Doppler linewidth. The fine structure of the 130.4 nm triplet is taken into account and the relative populations of the three fine levels of the ground states are assumed to follow a Boltzmann's distribution for both cold and hot oxygen populations. The distribution in the exosphere, where the collisions are negligible should be the distribution at the exobase if the typical travel time for one oxygen atom coming from the exobase and going back to the exobase is lower than the radiative time of the ground state. We estimate the travel time for an atom with a vertical velocity at the exobase ~3.9 km (reaching an altitude of 3500 km) to ~5000 s while the smallest radiation time is 11,000 s [*Froese Fischer and Saha*, 1983]. For the hot oxygen atoms, we have not investigated if a Boltzmann distribution at the kinetic hot temperature is valid. A better estimate would consist to solve the statistical distribution of each sublevel, taking into account the initial state of the atoms, the radiative time, ballistic time, and time between two collisions. It is beyond the scope of this paper to study such distribution.

The fine structure is needed to describe the relaxation of an excited atom toward the three different fine levels of the ground state according to the relative Einstein coefficients and, therefore, its contribution to the three lines of the triplet at 130.4 nm whatever the ground state of the atom before the scattering. When a photon is scattered by an oxygen atom, the new propagating direction of the photon is computed taking into account the phase function.

The phase function $p_i(\theta)$ of each line i of the 130.4 nm triplet is given by

$$p_i(\theta) = \left(1 - \frac{1}{4m_i}\right) + \frac{3}{4m_i}\cos^2\theta \tag{1}$$

where θ is the scattering angle and m_i an integer depending on the line of the triplet. From Table II, chapter 1 of Chandrasekhar [1960], we derive $m_1 = 100$, $m_2 = 4$, and $m_3 = 1$.

The wavelength of the scattered photon, taking into account the natural broadening of the lines, is derived from the algorithm presented in *Lee* [1982]. The test photon is then followed along its new direction and can be scattered again by some other oxygen atoms. The test photons are followed along their trajectory until they escape from Mars (upper boundary at 10,000 km) or are absorbed by CO_2.

For all the simulations performed in this study the total emission volume rate is divided in five emission volume rates corresponding to the following:
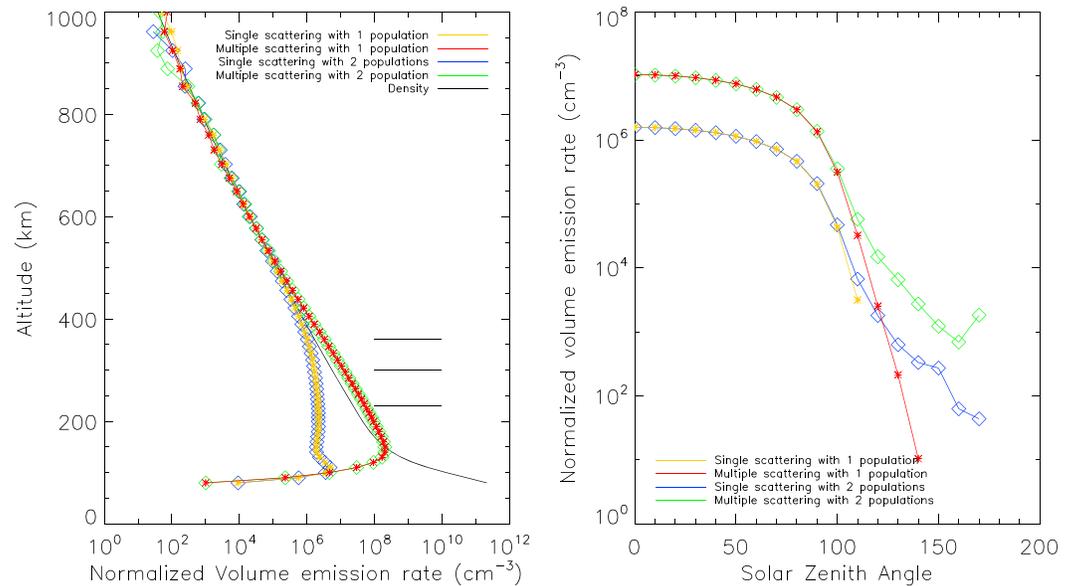
Figure 2. (left) Altitude profile of the single-scattering and multiple-scattering volume emission rate at SZA = 0° of the cold oxygen for a simulation without any hot populations and for a simulation with a hot oxygen density. The three horizontal black solid segments on Figure 2 (left) indicate approximately the altitude where the optical thickness at the center of each line of the O I 130.4 nm triplet is equal to 1. (130.2 nm ~ 360 km, 130.4 nm ~ 300 km, and 130.6 nm ~230 km). (right) Variations of the same volume emission rates with the solar zenith angle for an altitude near 300 km.

1. Single-scattering term for cold oxygen: solar photon scattered for the first time by a cold oxygen atom. Such photon could have been scattered by one or several hot oxygen atoms before.
2. Mutiple-scattering term for cold oxygen: solar photons scattered at least two times by a cold oxygen atom.
3. Single-scattering term for hot oxygen: solar photon scattered for the first time by a hot oxygen atom and never scattered before.
4. "Mars shine" scattering term for hot oxygen: solar photons already scattered by a cold oxygen and scattered for the first time by a hot oxygen.
5. Multiple scattering for hot oxygen: photons scattered at least two times by a hot oxygen atom.

All these terms are spectrally integrated and summed over the three lines of the 130.4 nm triplet.

The sum of the two first terms represent the total volume emission rate of the cold oxygen population and the sum of the three last terms the total volume emission rate of the hot oxygen population. All these terms are normalized by the solar g factor.

3. Effect of the Nonthermal Population on the Volume Emission Rate of the Thermal Population

In this section, we used the two populations radiative transfer model using the cold density profile represented by the green solid line in Figure 1 and the hot oxygen density profile represented by the green dashed line in Figure 1.

As shown in Figure 2, the dayside volume emission rate of the cold oxygen is not modified by the presence of a hot oxygen population. The slow decrease of the multiple scattering above the region where the optical thickness at the center of the line: $\tau = 1$ is due to the Mars shine effect discussed in detail in the next section.

In the nightside, as shown by Figure 2, the volume emission rate of the cold population is modified when a hot oxygen population is present. Indeed, solar photons cannot access directly the Martian shadow, so that only scattered photons can reach it. When an extended hot population is present around Mars, the number of photons scattered by this extended exosphere and reaching the shadow is not negligible and can even be dominant with respect to the photons scattered by the more compact cold oxygen exosphere. These
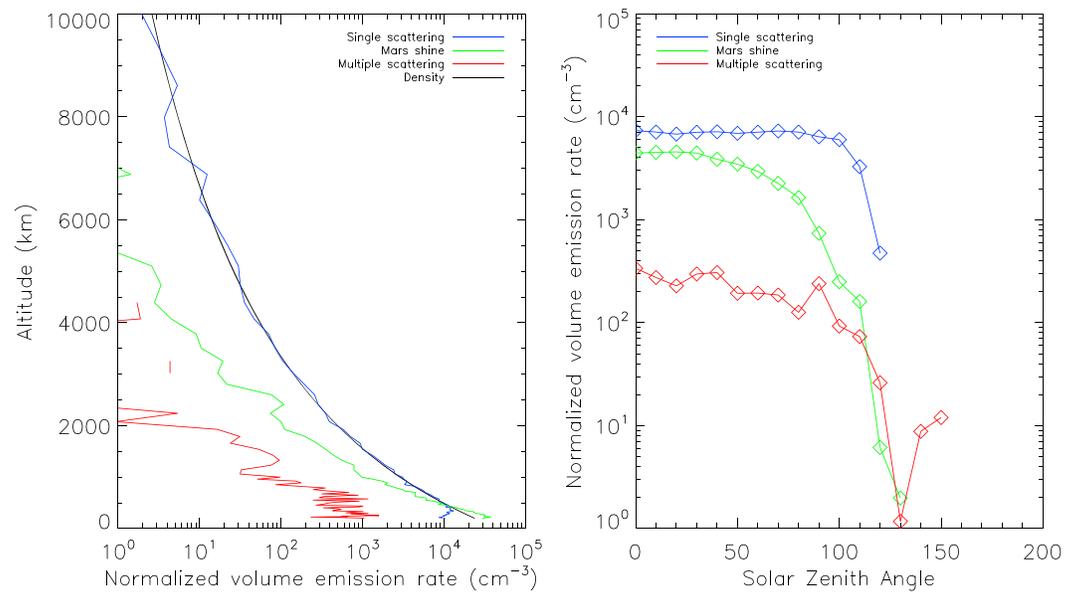
Figure 3. (left) Altitude profile of the single-scattering, "Mars shine" and multiple-scattering volume emission rates at SZA = 0° of the hot oxygen. (right) Variations of the same volume emission rates with the solar zenith angle for an altitude near 600 km.

photons increase the nightside volume emission rate of the cold oxygen corona. Therefore, our simulations suggest that observations of an emission at 130.4 nm at solar zenith angle (SZA) > 120° (depending on the altitude of the observations) could be interpreted as the evidence of a high-altitude oxygen-extended corona. At 200 km, the nightside volume emission rate is still ~4 orders of magnitude lower than the dayside volume emission rate, and therefore, the emission is difficult to detect.

4. Effect of the Thermal Population on the Volume Emission Rate of the Nonthermal Population

In this section, we investigate the effect of the cold oxygen population on the hot oxygen emission volume rate, in particular, any possible limitations of using only the primary sunlight source when interpreting the brightness of the high-altitude hot oxygen. The three components of the hot oxygen volume emission rates presented in section 2 against altitude and solar zenith angle are displayed in Figure 3.

Considering only the sunlight photons source would correspond to a normalized volume emission rate equal to the density (Figure 3). The simulated profiles of the volume emission rates are noisy due to the low numbers of scatterings in the Monte Carlo radiative transfer model. Below ~360 km, the departure between the single-scattering normalized term and the density is due to the effect of the total oxygen column density above that scatters the solar flux and therefore reduce the local solar flux.

The effect of the cold oxygen population on the volume emission rate of the hot oxygen is illustrated by the "shine" term. With our choice of cold oxygen density model, this term is dominant below 500 km and its effect decreases with altitude (Figure 3). At 4000 km, it only represents few percent of the total volume emission rate of the hot oxygen population. This term also decreases with solar zenith angle (Figure 3b) due to the decrease of the solar flux scattered by the cold oxygen population at large solar zenith angle. It is negligible in the shadow compared to the multiple-scattering term.

The dayside multiple-scattering term (due to the photons scattered several times by the hot oxygen population) is negligible at all altitudes for the hot oxygen density range shown in Figure 1. Only the terms with photons scattered one time by the hot population contribute to the total volume emission rate, and therefore, the Martian upper exosphere can still be considered as optically thin. As a consequence, the total volume emission rate should be proportional to the local hot oxygen density with a proportional factor depending only on the cold oxygen population.

The total volume emission rate of the hot oxygen population ε_{hot} can be written under the form

$$\varepsilon_{hot} = \varepsilon_0 + \varepsilon_{shine} = \left(g_{exc} + g_{shine,ph} + g_{shine,imp}\right) n_{hot} \tag{2}$$

where $\varepsilon_0 = g_{exc} n_{hot}$ is the single-scattering term, ε_{shine} is the contribution due to Mars shine: including the solar photons backscattered by the cold oxygen atoms in the thermosphere/lower exosphere ($g_{shine,ph} n_{hot}$) and the O 130.4 nm emissions produced by photoelectron impact on the cold oxygen atoms in the thermosphere ($g_{shine,imp} n_{hot}$).

The parameter g_{exc} is the excitation factor of the O 130.4 nm line depending on the solar flux given by

$$g_{exc} = \sqrt{\pi} F_T \sigma_0 \Delta\lambda_D \sum_j \gamma_j p_j \tag{3}$$

where F_T is the spectrally integrated solar flux of the 130.4 nm solar triplet, σ_0 is the cross section at the center of the line, identical for the three lines of the triplet due to the same values of the oscillator strengths [*Strickland and Donahue*, 1970], $\Delta\lambda_D$ the Doppler linewidth of one line taken identical for each line of the triplet, p_j is the relative population of the fine level j of the ground state, and γ_j, the ratio between the solar flux at the center of the solar line j Φ_{0j} and the total solar flux F_T. The parameters γ_j are derived from the solar spectral profiles given by *Gladstone* [1992]: $\gamma_1 = 1.18 \text{ Å}^{-1}$, $\gamma_2 = 1.43 \text{ Å}^{-1}$, and $\gamma_3 = 2.12 \text{ Å}^{-1}$. Due to the term in p_j and the fact that the solar lines have not the same flux Φ_{0j}, g_{exc} depends on the temperature. For the range of temperatures estimated for the hot oxygen temperature (1000–10,000 K), the variation of g_{exc} with the hot temperature is less than 5%.

We estimate the relative contribution of the photoelectron impact and solar photons to Mars shine, using the approach of *Strickland et al.* [1973] (see also *Chaufray et al.* [2009]) to describe the primary source of photons produced by photoelectron impact. We used an electron impact frequency of $8 \times 10^{-8} \text{ s}^{-1}$ at the top of the atmosphere of Mars [*Stewart et al.*, 1992] and a solar g factor of $5.7 \times 10^{-6} \text{ s}^{-1}$ [*Lee et al.*, 2015]. Using these values, we found for the oxygen density shown in Figure 2 that the contribution of the photoelectron impact ($g_{shine,imp}$) to the total shine term is 20% and the contribution of the solar photons ($g_{shine,ph}$) to the total shine term is 80% at SZA = 60°. The contributions of the photoelectron impact is 15% and 30% at SZA = 0° and 90°, respectively.

If we neglect the contribution of the photoelectron impact to the O 130.4 nm emission as source of Mars shine, then the volume emission rate of the hot oxygen is given by

$$\varepsilon_{hot} = \varepsilon_0 + \varepsilon_{shine,ph} = g_{exc}(1 + G_c) n_{hot} \tag{4}$$

G_c is a correction factor defined by

$$G_c = \frac{\varepsilon_{shine,ph}}{\varepsilon_0} = \frac{\varepsilon_{shine,ph}}{g_{exc} n_{hot}} \tag{5}$$

G_c depends on the cold oxygen population and therefore on the spatial position. For a spherically symmetric cold corona as used in these simulations, G_c is a function of the altitude and solar zenith angle only. When $G_c \ll 1$, the planet shine is negligible compared to the direct sunshine, and the volume emission rate is the product of the solar g factor and the hot oxygen density. At high altitudes where the slant optical thickness $\tau \ll 1$, the correction on the brightness along one line of sight is given by the integration of the volume emission rate:

$$I_{hot} = g_{exc} \int_s [1 + G_c(s)] n_{hot}(s) ds \tag{6}$$

The altitude variations of G_c for the two cold oxygen density profiles represented in Figure 1 by the black and red solid lines are displayed in Figure 4 at SZA = 0°. At SZA = 0°, the Mars shine can increase by more than 50% the full volume emission rate (and therefore brightness) at altitudes between 500 and 1000 km. G_c decreases with SZA and is lower than 1% at SZA > 110°. At high altitudes (above ~4000 km), G_c decreases as $1/r^2$ as expected from photons flux conservation (Figure 4), but at these altitudes, the effect is very small (<10%), lower than the noise of the IUVS data [*Deighan et al.*, 2015]. We performed simulations with the different hot oxygen profiles shown in Figure 1, to check if the G_c parameter is independent of the hot oxygen density profile as expected. Because the noise in the Monte Carlo simulations is reduced when using the denser hot oxygen model due to the larger number of scatterings, we used this model to estimate the variations of G_c with the altitude and solar zenith angle.
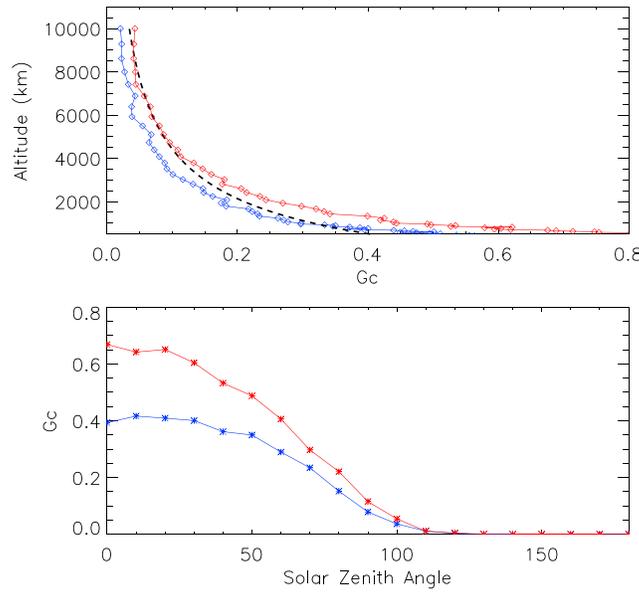
Figure 4. (top) G_c factor variations with altitudes for two different cold oxygen density profiles (see Figure 1) at SZA = 30°. The black dashed line represents the expected asymptotic variation in $1/r^2$. (bottom) G_c variations with SZA for the same density profiles near 750 km.

The estimated range of the G_c factor for SZA = 0°, 30°, 60°, and 90° at different altitudes, derived from this set of cold oxygen density models, are indicated in Table 1.

At SZA = 90°, the shine effect on the hot oxygen corona is small (<10% above 750 km) as also indicated in Figure 4.

The G_c factor depends also on the shape of the velocity distribution of the hot oxygen due to the dependence of the scatter cross section on this shape [e.g., *Chaufray and Leblanc*, 2013]. If the velocity distribution of the hot oxygen corona can be described by a Maxwellian distribution, G_c will depend on the kinetic temperature of the hot oxygen. MAVEN recent observations suggest that the hot oxygen population could be hotter than what was suggested from Alice/Rosetta observations. In Figure 5, we displayed the G_c factor for the same hot oxygen density model as in Figure 1, but assuming different kinetic temperatures for the hot oxygen atoms: $T_h = 2000$ K and $T_h = 8000$ K.

The G_c factor decreases with T_h due to the lower scattering cross section of the hot oxygen atoms ($\sigma_0 \sim T^{-1/2}$) near the spectral center of the lines corresponding to the wavelength of most of the backscattered photons by the cold oxygen atoms. If we assume that all photons are backscattered between $-3\Delta\lambda_{Dc}$ and $3\Delta\lambda_{Dc}$, where $\Delta\lambda_{Dc}$ is the Doppler wavelength at the cold kinetic temperature T_c, and if we neglect the scatterings by the Lorentzian wings of the Voigt profile, then the efficiency of the shine effect on the hot oxygen should be proportional to the hot oxygen scattering cross section integrated over this wavelength range, i.e., H given by

$$H = \int_{-3\sqrt{\frac{T_c}{T_h}}}^{3\sqrt{\frac{T_c}{T_h}}} e^{-x^2}\mathrm{d}x = \sqrt{\pi}\mathrm{erf}\left(3\sqrt{\frac{T_c}{T_h}}\right) \qquad (7)$$

where T_h is the kinetic temperature of the hot oxygen distribution and erf the error function. The G_c values derived at $T_h = 2000$ K and rescaled by $H(T_h = 8000$ K$)/H(T_h = 2000$ K$)$ are also displayed in Figure 5, showing a good agreement with the G_c values derived for $T_h = 8000$ K. Such a scaling has been found to work well for $T_c = 300$ K and $T_h = 2000$ K, 4000 K, 6000 K, and 8000 K. Therefore, the values given in Table 1 ($T_h = 2000$ K) can be rescaled for other values of the hot kinetic temperature. For $T_h \gg T_c$, H varies as $T_h^{-1/2}$ as expected from the variation of the scattering cross section at the center of the lines. Because G_c depends on the cold oxygen density, these values cannot be rescaled directly for different cold oxygen temperatures due to the dependence on the cold density scale height with this temperature.

5. Conclusion

We used a radiative transfer model including cold and hot oxygen populations in the Martian exosphere, as

Table 1. Range of the G_c Factor for Different SZA and Different Altitudes for Th = 2000 K Computed Using the Cold Oxygen Density Profiles Represented by the Black and Red Solid Lines on Figure 1

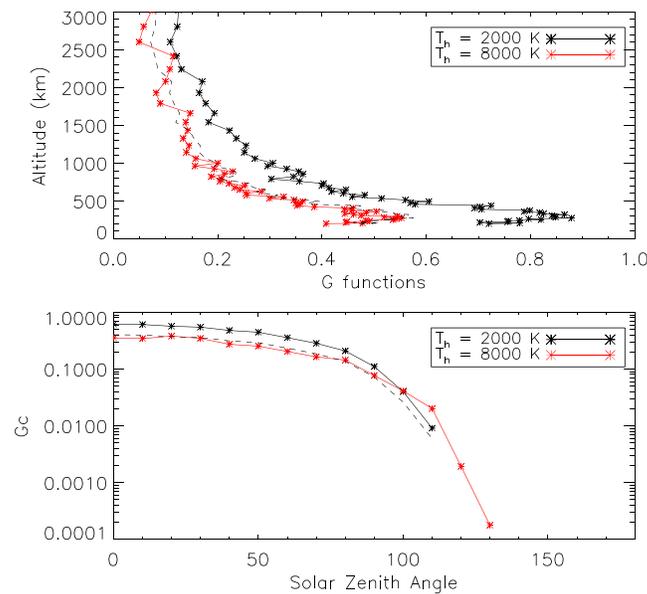| Altitude\SZA	0°	30°	60°	90°
500 km	0.5–0.9	0.5–0.9	0.4–0.6	0.1–0.2
750 km	0.4–0.7	0.4–0.6	0.3–0.4	0.08–0.1
1000 km	0.4–0.5	0.3–0.4	0.2–0.3	0.07–0.09
1500 km	0.3–0.4	0.2–0.3	0.1–0.2	0.06–0.08
2000 km	0.2–0.3	0.2–0.25	0.1–0.2	0.04–0.06
3000 km	0.1–0.2	0.1–0.2	0.08–0.1	0.04–0.05

Figure 5. (top) Altitude profile of the G_c function for the same cold and hot oxygen density profiles but for the different velocity distribution shape of the hot oxygen population defined by $T_h = 2000$ K (black solid line) and $T_h = 8000$ K (red solid line). The dashed black line corresponds to the profile with $T_h = 2000$ K rescaled to 8000 K using the scaling factor H defined by equation (3). (bottom) SZA profile of the G_c function for the same cold and hot oxygen density profiles but for the different velocity distribution shape of the hot oxygen population defined by $T_h = 2000$ K (black solid line) and $T_h = 8000$ K (red solid line). The dashed black line corresponds to the profile with $T_h = 2000$ K rescaled to 8000 K using the scaling factor H defined by equation (3).

recently observed by MAVEN, to investigate the effect of Mars shine on the volume emission rate of the hot oxygen corona. While the volume emission rate of the thermal oxygen population is affected by the presence of a suprathermal population only on the nightside hemisphere, the volume emission of the dayside hot oxygen rate mainly due to the solar resonant scattering can be increased by about 50% when Mars shine is included (i.e., the g factor should be increased by about 50%) depending on the spatial position. While neglecting Mars shine is sufficient to already provide strong constraints on the origin of the hot oxygen corona, any accurate estimate of the hot oxygen corona and associated escape rate will need to take it into account. Because of the expected temporal variations of the oxygen density in the thermosphere/exosphere resulting, for example, from the large temporal variability of the exospheric temperature [*Gonzalez-Galindo et al.*, 2015], this effect will be time vari-able. While taking into account that this effect will slightly improve the comparisons between the IUVS observations and the simulations performed by *Lee et al.* [2015], it cannot explain alone the observed systematic discrepancy. Indeed, such discrepancy would require too large cold oxygen densities in the thermosphere/exosphere or unrealistically low kinetic temperature for the hot oxygen population. This effect is not uniform and acts to reduce the brightness scale height, so that the temperature derived from the scale height of the brightness of the hot corona would be underestimated.

References

Bougher, S., et al. (2015), Early MAVEN Deep Dip campaign reveals the thermosphere and ionosphere variability, *Science*, *350*, 6261, doi:10.1126/science.aad0459.

Carveth, C., J. T. Clarke, J.-Y. Chaufray, and J.-L. Bertaux (2012), Analysis of HST spatial profiles of oxygen airglow from Mars, B.A.A.S., 2012DPS....4421403C.

Chamberlain, J. W. (1963), Planetary coronae and atmospheric evaporation, *Planet. Space Sci.*, *11*, 901–960, doi:10.1016/0032-0633(63)90122-3.

Chandrasekhar, S. (1960), *Radiative Transfer*, Dover Publ. Inc., New York.

Chaufray, J.-Y., and F. Leblanc (2013), Radiative transfer of emission lines with non-Maxwellian velocity distribution function: Application to Mercury D2 sodium lines, *Icarus*, *223*, 975–985, doi:10.1016/j.icarus.2013.01.005.

Chaufray, J.-Y., R. Modolo, F. Leblanc, G. Chanteur, R. E. Johnson, and J. G. Luhmann (2007), Mars solar wind interaction: Formation of the Martian corona and atmospheric loss to space, *J. Geophys. Res.*, *112* E09009, doi:10.1029/2007JE002915.

Chaufray, J.-Y., F. Leblanc, E. Quémerais, and J.-L. Bertaux (2009), Martian oxygen density at the exobase deduced from O I 1304 nm observations by SPICAM on Mars Express, *J. Geophys. Res.*, *114* E02206, doi:10.1029/2008JE003130.

Chaufray, J.-Y., et al. (2015a), Study of the Martian cold oxygen corona from the O I 130.4 nm line by IUVS/MAVEN, *Geophys. Res. Lett.*, *42*, 9031–9039, doi:10.1002/2015GL065341.

Chaufray, J.-Y., J.-L. Bertaux, E. Quémerais, F. Leblanc, and S. Sulis (2015b), Observations of the nightside Venusian hydrogen corona with SPICAV/VEX, *Icarus*, *262*, 1–8, doi:10.1016/j.icarus.2015.08.013.

Deighan, J., et al. (2015), MAVEN IUVS observation of the hot oxygen corona at Mars, *Geophys. Res. Lett.*, *42*, 9009–9014, doi:10.1002/2015GL065487.

Feldman, P. D., et al. (2011), Rosetta-Alice observations of exospheric hydrogen and oxygen on Mars, *Icarus*, *214*, 394–399, doi:10.1016/j.icarus.2011.06.013.

Froese Fischer, C., and H. P. Saha (1983), Multiconfiguration Hartee-Fock results with Breit-Pauli corrections for forbidden transitions in the 2p[4] configuration, *Phys. Rev. A*, *28*, 3169–3178, doi:10.1103/PhysRevA.28.3169.

Gladstone, G. R. (1992), Solar OI 1304-A triplet line profiles, *J. Geophys. Res.*, *97*, 19,519–19,525, doi:10.1029/92JA00991.

Gonzalez-Galindo, F., F. Forget, M. A. López-Valverde, M. Angelats i Coll, and E. Millour (2009), A ground-to-exosphere Martian circulation model: 1. Seasonal, diurnal and solar cycle variation of thermospheric temperatures, *J. Geophys. Res.*, *114* E04001, doi:10.1029/2008JE003246.

Gonzalez-Galindo, F., M. A. Lopez-Valverde, F. Forget, M. Garcia-Comas, E. Millour, and L. Montabone (2015), Variability of the Martian thermosphere during eight Martian years as simulated by a ground-to-exosphere global circulation model, *J. Geophys. Res. Planets*, *120*, 2020–2035, doi:10.1002/2015JE004925.

Groller, H., H. Lichtenegger, H. Lammer, and V. I. Shematovich (2014), Hot oxygen and carbon escape from the Martian atmosphere, *Planet. Space Sci.*, *98*, 93–105, doi:10.1016/j.pss.2014.01.007.

Hanson, W. B., S. Satani, and D. R. Zuccaro (1977), The Martian ionosphere as observed by the Viking retarding potential analyzers, *J. Geophys. Res.*, *82*, 4351, doi:10.1029/JS082i028p04351.

Krasnopolsky, V. (2002), Mars' upper atmosphere and ionosphere at low, medium, and high solar activities: Implications for evolution of water, *J. Geophys. Res.*, *107*(E12), 5128, doi:10.1029/2001JE001809.

Leblanc, F., et al. (2015), Mars heavy ion precipitating flux as measured by Mars Atmosphere and Volatile EvolutioN, *Geophys. Res. Lett.*, *42*, 9135–9141, doi:10.1002/2015GL066170.

Lee, J.-S. (1982), Refined Monte Carlo method for simulating angle-dependent partial frequency redistributions, *Astrophys. J.*, *255*, 303–306, doi:10.1086/159829.

Lee, Y., M. R. Combi, V. Tenishev, S. W. Bougher, J. Deighan, N. M. Schneider, W. E. McClintock, and B. M. Jakosky (2015), A comparison of 3-D model predictions of Mars' oxygen corona with early MAVEN IUVS observations, *Geophys. Res. Lett.*, *42*, 9015–9022, doi:10.1002/2015GL065291.

McElroy, M. B. (1972), Mars: An evolving atmosphere, *Science*, *175*, 443–445, doi:10.1126/science.175.4020.443.

Nagy, A. F., T. E. Cravens, J. H. Lee, and A. I. F. Stewart (1981), Hot oxygen atoms in the upper atmosphere of Venus, *Geophys. Res. Lett.*, *8*, 629–632, doi:10.1029/GL008i006p00629.

Stewart, A. I. F., M. J. Alexander, R. R. Meier, L. J. Paxton, S. W. Bougher, and C. G. Fesen (1992), Atomic oxygen in the Martian thermosphere, *J. Geophys. Res.*, *97*, 91–102, doi:10.1029/91JA02489.

Strickland, D. J., and T. M. Donahue (1970), Excitation and radiative transport of OI 1304 A resonance radiation: I The dayglow, *Planet. Space Sci.*, *18*, 661–689, doi:10.1016/0032-0633(70)90049-8.

Strickland, D. J., A. I. Stewart, C. A. Barth, C. W. Hord, and A. L. Lane (1973), Mariner 9 ultraviolet spectrometer experiment: Mars atomic oxygen 1304-A emission *J. Geophys. Res.*, *78*, 4547–4559, doi:10.1029/JA078i022p04547.

Valeille, A., V. Tenishev, S. W. Bougher, M. R. Combi, and A. F. Nagy (2009a), Three-dimensional study of Mars upper thermosphere/ionosphere and hot oxygen corona: 1. General description and results at equinox for solar low conditions, *J. Geophys. Res.*, *114* E11005, doi:10.1029/2009JE003388.

Valeille, A., M. R. Combi, S. W. Bougher, V. Tenishev, and A. F. Nagy (2009b), Three-dimensional study of Mars upper thermosphere/ionosphere and hot oxygen corona: 2 Solar cycle, seasonal variations, and evolution over history, *J. Geophys. Res.*, *114*, E11006, doi:10.1029/2009JE003389.

Yagi, M., F. Leblanc, J.-Y. Chaufray, F. Gonzalez-Galindo, S. Hess, and R. Modolo (2012), Mars exospheric thermal and non-thermal components: Seasonal and local variations, *Icarus*, *221*, 682–693, doi:10.1016/j.icarus.2012.07.022.